

An AGN Sample with High X-ray-to-optical Flux Ratio from RASS

II. Optical Emission Line Properties of Seyfert 1 Type AGN

D. W. Xu^{1,2}, Stefanie Komossa², J. Y. Wei¹, Y. Qian³ and X.Z. Zheng¹

ABSTRACT

This work studies the optical emission line properties of a sample of 155 low-redshift bright X-ray selected ROSAT Seyfert 1 type AGN for which adequate signal-to-noise ratio spectroscopic observations are available. We measured emission line properties by performing multi-component fits to the emission line profiles, covering the effect of blended iron emission. We also obtained continuum parameters, including 250eV X-ray luminosities derived from the ROSAT database. In addition, the measured properties are gathered for a correlation analysis, which confirms the well-known relations between the strengths of Fe II, [O III] emission and the X-ray slope. We also detect striking correlations between H β redshift (or blueshift), flux ratios of Fe II to H β broad component and [O III] to H β narrow component. These trends are most likely driven by the Eddington ratio.

Subject headings: Galaxies: Seyfert – Quasars: emission lines – X-rays: galaxies

1. Introduction

Optical spectra of Active Galactic Nuclei (AGN) exhibit an extremely wide variety of properties. The emission-line regions of AGN have proven to be among the most complex of all astrophysical environments (Corbin & Boroson 1996). AGN have also been known to emit a substantial fraction of their luminosity as X-rays. Multi-wavelength observations of well-defined source samples are effective in understanding the physical processes in AGN.

¹National Astronomical Observatories, Chinese Academy of Sciences, Beijing 100012, China; dwxu@bao.ac.cn, wjy@bao.ac.cn, zxz@alpha.bao.ac.cn

²Max-Plank-Institut für extraterrestrische Physik, Postfach 1312, D-85741 Garching, Germany; dwxu@mpe.mpg.de, skomossa@mpe.mpg.de

³Department of Physics, Tsinghua University, Beijing 100080, China

In the last decade, several correlations between optical emission line properties and X-ray properties were noted (Boroson & Green 1992; Lawrence et al. 1997; Grupe et al. 1999; Vaughan et al. 2001): for instance, the strong correlations between optical Fe II, [O III] λ 5007 line strengths, velocity width of H β and the slope of soft X-ray continuum (α_X). These correlations received great interest previously and were expected to give important insight into the AGN phenomenon. Still, however, their interpretation remained unclear. It is therefore of great importance to test whether these correlations are fundamental properties or subtle selection effects, and search for new ones. Clearly, a large and homogeneous X-ray selected sample would be advantageous in addressing these issues. We present such a sample here.

X-ray AGN samples are also of great interest for a number of other issues. AGN of different types are the major contributors to the extragalactic soft and hard X-ray background (XRB). The definitions of statistically significant AGN samples using X-ray data are key to test AGN number-flux relations, luminosity functions and cosmological evolution. In the course of the ROSAT All Sky Survey (RASS) (Voges et al. 1996, 1999), many new AGN have been identified by different teams, confirming that X-ray surveys are very efficient in finding new AGN. Schwope (2000) performed an unbiased survey of all bright, $CR > 0.2 \text{ s}^{-1}$, high galactic latitude sources in the RASS without applying other selection criteria. Wei et al. (1999, Paper I) identified a sample with high X-ray to optical flux ratio. Appenzeller et al. (1998) and Zickgraf et al. (1997) presented a catalog of sources in selected areas down to the RASS limit. Thomas et al. (1998) drew a high galactic latitude sample from the RASS with soft PSPC spectra ($HR1 < 0.0$), the corresponding sample of point-like X-ray sources with relatively hard X-ray spectra ($HR1 > 0.5$) was presented by Fischer et al. (1998). Bade et al. (1995, 1998) published a catalog of northern AGN in the RASS based on their Schmidt plate survey. These authors presented new AGN, but they did not use their samples to address correlations issues. This will be done with the present sample.

In Paper I we described and presented the optical identification of a sample of 165 X-ray sources with high X-ray to optical flux ratio (f_X/f_{opt}) discovered in the RASS. About 73% of the sources were identified as AGN, including 115 emission line AGN (QSOs and Seyferts) as well as 2 BL Lac objects and 4 BL Lac candidates. In this paper we investigate the optical emission line properties of the emission line AGN that were identified as main optical counterparts of the sample and discuss their connection with X-ray properties. Not included in the following discussion are the BL Lac objects.

The initial identification program excluded known X-ray sources that have counterparts in the SIMBAD, NED and AGN catalogs. Motivated by the need of larger and better samples, we have cross-referenced the RASS bright source catalog with the NED and AGN

catalogs. We find that 40 known emission line AGN meet our selection criteria.⁴ In order to keep consistent emission line properties measurements, new optical spectra have been acquired for the 40 additional sources. These data, combined with the previous optical identifications, provide a large, bright and (f_X/f_{opt}) limited sample of emission line AGN in the ROSAT X-ray band. The relatively complete sample is the largest X-ray selected AGN sample with intense optical investigation so far.

As described in Paper I, our classifications and identifications were based on low resolution spectra obtained with a 2.16 m telescope at Xinglong station, National Astronomical Observatories of China (NAOC). These spectra were exposed to reach a S/N suitable for a reliable classification. The quality of the majority spectra is sufficient to measure the properties of the emission lines, such as the line widths and line strengths. For spectra with inadequate S/N, new low resolution ($\sim 10\text{\AA}$ FWHM) optical spectroscopy was performed using the 2.16 m telescope at NAOC.

All objects in our emission line AGN subsample are found to be Seyfert 1 type AGN. Throughout this paper Seyfert 1 galaxies and QSOs will be discussed jointly, since these two classes are distinguished only by a certain luminosity level according to our classification criterion. We do not divide the Seyfert 1 class into subclasses such as Seyfert 1.5-1.9 or NLS1 galaxies (as defined by Véron-Cetty & Véron (2000), Osterbrock & Pogge (1985)), since the definitions of Seyfert classifications depend on the resolution of the spectra used and the noise in the spectra (Grupe et al. 1999; Goodrich 1989a,b).

The paper is organized as follows. Detailed optical measurements are given in Sect. 2. The statistical properties are investigated in Sect. 3. Several diagnostically important correlations that exist between emission line and continuum properties are studied. Sect. 4 discusses the implications of the results, followed by a brief summary of the main conclusions of the paper.

Throughout this paper, a Hubble constant of $H_0 = 50 \text{ km s}^{-1} \text{ Mpc}^{-1}$ and a deceleration parameter of $q_0 = 0$ are assumed and all measured parameters are quoted for the rest frame of the source.

⁴The selection criteria of the sample are: an alternative high X-ray-to-optical flux ratio criterion, i.e., $\log \text{CR} \geq -0.4 \text{ R} + 4.9$, where CR and R represent X-ray count rate and R magnitude respectively; declination $\delta \geq 3^\circ$; galactic latitude $|b| \geq 20^\circ$; optical counterparts within a circle with radius $r = r_1 + 5''$, where r_1 is the RASS position error given by Voges et al.(1996); optical counterparts with R magnitudes between 13.5 and 16.5.

2. Observations and Optical Measurements

2.1. New Optical Observations

The known sources as well as sources without high quality observations in the identification campaign were investigated during several observing runs performed from November 1998 through December 2000. The low resolution spectra were taken with the NAOC 2.16 m telescope and the OMR spectrograph, using a Tektronix 1024×1024 CCD as detector. The grating of 300 g mm^{-1} was employed in order to get large wavelength coverage. All observations were made through a $2.3''$ slit that produced a resolution of 10 to 11\AA as measured from the comparison spectra. This set-up provided similar wavelength coverage ($3800\text{\AA} - 8200\text{\AA}$) and resolution to the identification data. Exposure time was generally between 1200s and 3600s depending on the brightness of the object. For a few objects, multiple exposures were performed in order to get a higher S/N spectrum. The exposures were combined prior to extraction where possible in order to help remove cosmic ray contamination. In cases when the target source moved across the CCD chip between exposures, the data were extracted separately from each frame and then combined.

The raw data were reduced following standard procedures using IRAF. The CCD reductions included bias subtraction, flatfield correction and cosmic-ray removal. Wavelength calibration was carried out using helium-neon-argon lamps taken at the beginning and end of each exposure. The resulting wavelength accuracy is better than 1 \AA . The flux calibration was derived with 2 to 3 observations of KPNO standard stars (Massey & Strobel 1988) per night.

2.2. Fe II Subtraction

In many of the spectra there is a clear contribution from blends of Fe II line emission on both the blue and red sides of the $\text{H}\beta$ -[O III] complex. These blends contaminate strong lines such as [O III] $\lambda\lambda 4959, 5007$, and may alter the flux and width of $\text{H}\beta + [\text{O III}] \lambda\lambda 4959, 5007$. In order to reliably measure line parameters and to determine the strength of the Fe II emission, we have carefully removed the Fe II multiplets following the method described by Boroson & Green (1992), which relies on an Fe II template. The template used in the present work is the same as that of Boroson & Green (1992), namely the Fe II lines of I Zw 1, a bright NLS1 widely known for the strong and narrow permitted Fe II emission (Phillips 1978; Oke & Lauer 1979). The observed spectra were wavelength-shifted to the rest frame according

to the redshift.⁵ The whole template was broadened to the FWHM of the broad $H\beta$ line by convolving with a Gaussian and scaled to match the line intensities. The best match was then searched for in the two-dimensional parameter space of line width and line strength. From each object the best-fit Fe II spectrum was then subtracted. A successful Fe II subtraction showed a flat continuum between the $H\gamma$ and $H\beta$ and between 5100–5400Å (which covers the Fe II multiplets 48, 49). The Fe II flux was measured between the rest wavelength 4434Å and 4684Å as in Boroson & Green (1992).

2.3. Other Line Measurements

The characteristic property of Seyfert 1 type AGN is the presence of broad emission lines. The line widths and their distributions provide important information on masses of the central black holes and mass distributions. The broad Balmer lines in AGN exhibit a wide variety of profile shapes and a large range in width (Osterbrock & Shuder 1982; de Robertis 1985; Cresshaw 1986; Stripe 1991; Miller et al. 1992; Véron-Cetty, Véron & Gonçalves 2001) and they are often strongly asymmetric (Corbin 1995). In many cases $H\beta$ is a mixture of broad and narrow components. Differences in the relative strengths of these components account for much of the diversity of broad line profiles (Francis et al. 1992; Wills et al. 1993; Brotherton et al. 1994; Corbin 1995, 1997; Véron-Cetty, Véron & Gonçalves 2001).

The Fe II subtracted spectra were used to measure the non-Fe II line properties. In order to isolate the broad $H\beta$ component in all spectra, we have assumed that the emission line profiles can be represented by a single or a combination of Gaussian profiles. Véron-Cetty, Véron & Gonçalves (2001) claimed that the broad emission lines in NLS1 galaxies were better fitted with Lorentzian profiles than with Gaussian profiles. However, as noted in Evans (1988), the choice of Gaussian or Lorentzian profiles as representatives of the observed emission lines may bear no physical meaning. We performed a multiple Gaussian fit in the present work for its simplicity and a direct comparison with the measurements of previous studies (e.g. Boroson & Green (1992); Grupe et al. (1999); Vaughan et al. (2001)). We adopted the method described by Rodríguez-Ardila et al. (2000b) and used the IRAF package SPECFIT⁶ to measure blended lines. As a first step we tried to fit the emission lines with a single Gaussian component. It worked well for most forbidden lines, e.g., $[O\ III]\lambda 5007$. However, this simplest representation could not fit adequately the wings

⁵We take the redshift from $[O\ III]\lambda 5007$ to be the systemic redshift as most commonly used. The redshift was derived from fitting a Gaussian to the upper half of the observed $[O\ III]\lambda 5007$ line in each spectrum.

⁶SPECFIT is developed and kindly provided by Dr. G. Kriss.

of $H\beta$, although its core was nicely fitted in most of targets. In such cases, we then included one narrow component and one broad component to describe adequately the observed profile. (Note that when $H\beta$ measurements were taken from the literature, many of them refer to the whole line.) For each assumed component, a first guess of the central wavelength, the total flux, and width of that component were specified. There were two parameters for each continuum component, i.e., the flux and the slope. Initially, we constructed a narrow component with a width determined from fitting the [O III] lines. In some spectra such a guess failed to give a good fit and needed an additional component. We then left the width of the narrow component as a free parameter. It led to a nice fitting result by checking the residual, i.e., the narrow component could be well isolated from the broad component. For $H\beta$ lines with asymmetric profile, the two Gaussian components are not stationary in wavelength. The velocity shift between the broad and narrow components is defined as the shift of the broad component relative to the narrow component in units of km s^{-1} (see also Zheng et al 2002). As an illustration, we show the decomposition in Figure 1. The observed profile is represented by a solid line, the total fit by a dashed line, the individual Gaussian components by a dot-dashed line and the differences between the data and the fit (the residual) by the lower dotted line.

The broad component is referred as $H\beta_b$, and the narrow component as $H\beta_n$. The FWHM $H\beta_b$ is what we consider as representative of the Broad Line Region (BLR). The instrumental resolution was determined from the FWHMs of night sky spectra taken with each of the exposures and tested by comparison-lamp spectra. All quoted line widths were corrected for the instrumental resolution. The uncertainty of $H\beta$ velocity shift measurement is within 150 km s^{-1} . To measure line fluxes and equivalent widths (EW), power-law continua were fitted and subtracted from underneath the lines and the remaining line flux was integrated. For most objects, the uncertainty of flux measurement of emission lines is about 10% to 15%.

2.4. Continuum Measurements

The continuum level at the position of $H\beta \lambda 4861$ was measured from the Fe II subtracted spectra. All equivalent widths measurements in this paper refer to the continuum at that point to allow direct comparison with the measurements for other samples (Boroson & Green 1992; Grupe et al. 1999; Vaughan et al. 2001). The optical index α_{opt} was calculated using the continuum flux density at 4000\AA and 7000\AA in the rest frame.

For the X-ray analysis, a single power law description was employed. This application has proven to be a fairly good approximation for AGN in previous studies (e.g. Fiore et

al. 1994, Brinkmann & Siebert 1994, Schartel et al. 1996, Grupe et al. 1998). Because of the limited signal-to-noise ratio of the RASS spectra we assumed that the absorption comes from our Galaxy only. The assumption usually improves the reliability of the estimation of spectral index because of the reduced number of free parameters. The X-ray spectral slope $\alpha_X (F_\nu \propto \nu^{-\alpha})$ was estimated using the ROSAT hardness ratios HR1 and HR2, which are defined as (Voges et al. 1999):

$$\text{HR1} = \frac{B - A}{B + A}$$

$$\text{HR2} = \frac{D - C}{D + C}$$

Here, A, B, C and D denote the count rate in the energy range 0.1–0.4 keV, 0.5–2.0 keV, 0.5–0.9 keV and 0.9–2.0 keV, respectively.

3. Analysis

3.1. General Sample Properties

The full optical dataset was used to define the statistical properties of the sample and explore the correlations between various observed parameters. According to Paper I, 115 sources (about 73% of the total) were identified as new Seyfert 1s and QSOs, together with 40 known emission line AGN that meet our sample selection criteria, the AGN subsample comprises 49 “ultrasoft” ($\alpha_X > 1.7$) sources and 106 “normal” objects with mean $\langle \alpha_X \rangle = 1.43$. In the catalog in Paper I we listed the absolute magnitude M_B and redshift z . The distributions of the M_B values and redshift are plotted in Figure 2. As shown by these figures, the sample is dominated by moderate luminosity objects ($M_B \approx -23 \pm 2$) with an average redshift $\langle z \rangle = 0.2$.

Table 1 lists the derived parameters. The columns list the following information: (2) redshift; (3) FWHM of broad $H\beta$; (4) FWHM of narrow $H\beta$; (5) FWHM of $[O\ III]\lambda 5007$; (6), (7) and (8) the local equivalent widths of $H\beta$ broad component, Fe II and $[O\ III]\lambda 5007$; (9) and (10) ratio of fluxes of $[O\ III]\lambda 5007$ to broad and narrow $H\beta$; (11) ratio of fluxes of Fe II to broad $H\beta$; (12) velocity shift between $H\beta$ broad and narrow components, where a positive velocity corresponds to a redshifted broad component relative to narrow component; (13) and (14) $H\beta$ broad and narrow components velocity shift with respect to the systemic frame, where a positive velocity indicates a redward shift with respect to systemic; (15) and (16) spectral indices defined above; (17) the monochromatic 250eV luminosity.

The distribution of the broad $H\beta$ line width of the objects in our emission line AGN subsample shows a significantly smaller fraction (3%) of objects with $\text{FWHM} < 2000 \text{ km s}^{-1}$

compared to another X-ray selected sample (18%) (Appenzeller et al. 2000). However, the FWHM measurements in Appenzeller et al. (2000) refer to the full line profile and the widths of the broad components may have been underestimated. Therefore, the real difference should be smaller. Five out of 155 objects in our sample are NLS1 galaxies without detectable broad Balmer line components of $\text{FWHM} > 2000 \text{ km s}^{-1}$ but with strong Fe II emission, which agrees within the error limits with that of Appenzeller et al. (2000) (about 2%). The distribution of the FWHM of the broad component of $\text{H}\beta$ in the sample is displayed in Figure 3. The mean value of 4350 km s^{-1} is similar to the hard sample of Grupe et al. (1999).

3.2. Distribution of Velocity Shifts

The velocity shift distribution of $\text{H}\beta_b$ with respect to $[\text{O III}]\lambda 5007$ is shown in Figure 4a. Positive velocity corresponds to a redward $\text{H}\beta$ with respect to systemic, while a negative velocity represents a blueshift. The peak of this distribution is near zero, but has a mean redshift of 78 km s^{-1} with standard deviation of 305 km s^{-1} . This shift is in good agreement with the previous studies (Gaskell 1982; Tytler & Fan 1992; Boroson & Green 1992; Laor et al. 1995; Corbin & Boroson 1996), i.e., Balmer emission lines gives the same redshift to within 100 km s^{-1} of narrow forbidden emission (*e.g.* $[\text{O III}]\lambda 5007$) in low redshift ($z < 1$) QSOs and Seyfert galaxies. In contrast, a systematic mean redward shift of 520 km s^{-1} was found for a high redshift ($2.0 \lesssim z \lesssim 2.5$) QSOs sample (McIntosh et al. 1999). McIntosh et al. (1999) proposed this observed trend of increased Balmer redshift with increased systemic redshift represents a luminosity dependency.

For comparison, we also present the $\text{H}\beta_n - [\text{O III}]\lambda 5007$ shift in Figure 4b. The mean of the distribution is 8 km s^{-1} with a standard deviation of 176 km s^{-1} . We can see from the figures that the dispersion of the $\text{H}\beta_n - [\text{O III}]\lambda 5007$ shift is significantly narrower than the $\text{H}\beta_b - [\text{O III}]\lambda 5007$ shift, which is expected by the different emitting regions between $\text{H}\beta$ broad component and narrow component, as well as $[\text{O III}]\lambda 5007$.

In a similar manner to the $\text{H}\beta_b - [\text{O III}]\lambda 5007$ shift, Figure 4c illustrates the velocity differences between the broad and narrow components of $\text{H}\beta$. The redshift (or blueshift) is defined as the shift of the broad component relative to the narrow component in units of km s^{-1} . Positive velocities refer to redshifts with respect to the narrow component velocities, whereas negative velocities indicate blueshifts. We emphasize that both the $\text{H}\beta$ redshift (or blueshift) in the present work and the asymmetry parameter in Boroson & Green (1992) are measures for line profile, but characterized differently. The latter is a measure of the shift between the centroids at $1/4$ and $3/4$ maximum. The mean redshift of the distribution

is found to be 70 km s^{-1} with a standard deviation of 357 km s^{-1} . Correlation analyses involving the line profiles of $\text{H}\beta$ are investigated in section 3.3.

3.3. Correlations Analysis

In this subsection, we explore whether the various emission-line and continuum properties correlate with one another. For this purpose, we calculated the Spearman rank-order correlation matrix (Press et al. 1992), along with its significance matrix for measured properties. The complete correlation coefficient matrix is shown in Table 2. The number of parameter pairs included in the trials ranges from 86 to 149. Spectra with $\text{S/N} < 10$ were excluded from the analyses including optical properties. The probability of the null correlation, Ps , for a sample with corresponding correlation coefficient Rs is also given in Table 2 for entries with $\text{Ps} < 0.01$. A set of 12 different properties results in $12 \times (11/2) = 66$ correlation coefficients; therefore, at this level of significance, we would expect $\lesssim 1$ spurious events.

Among 66 trials, 31 correlations (both positive and negative) are found with two-sided probabilities $\text{Ps} < 0.01$. Four are due to the dependent parameters, e.g., relative strength of Fe II to $\text{H}\beta$ and Fe II EW; 12 are degenerate correlations, i.e., different measures of the same property (e.g., $[\text{O III}] \text{ EW}$, $[\text{O III}]/\text{H}\beta_b$ and $[\text{O III}]/\text{H}\beta_n$) all correlate with another property (e.g., Fe II EW); and therefore 15 are independent correlations at the $\gtrsim 99\%$ confidence level.

The well-known anti-correlation between the X-ray spectral slope α_X and the FWHM of $\text{H}\beta$ (Boller et al. 1996; Laor et al. 1997; Grupe et al. 1999) is not prominent in our sample ($\text{Rs} = -0.20$, $\text{Ps} = 0.05$) as is the case in the Vaughan et al. (2001) sample ($\text{Rs} = -0.31$, $\text{Ps} = 0.03$). Vaughan et al. (2001) suggested that the relation between $\text{H}\beta$ width and α_X is not a linear correlation, but probably resulted from a “zone of avoidance” (Komossa et al. 2001), i.e., broad line objects always tend to show flat X-ray spectra, whereas there is a very large scatter in the X-ray spectral steepness of NLS1 galaxies, with several as flat as normal Seyfert 1s (Xu et al. 1999). The correlation is more pronounced among the AGN with higher luminosity as in the samples of Grupe et al. (1999) and Vaughan et al. (2001). For objects with $\nu\text{L}_{250\text{eV}} > 10^{44.3} \text{ erg s}^{-1}$ the significance becomes $\text{Rs} = -0.45$ ($\text{Ps} = 0.007$). The correlation between α_X and $\text{H}\beta_b$ is illustrated in Figure 5.

The anti-correlation between the width of $\text{H}\beta$ and Fe II/ $\text{H}\beta$ (Wills 1982; Boroson & Green 1992; Wang, Brinkmann, & Bergeron 1996; Rodríguez-Ardila et al. 2000a) is strong ($\text{Rs} = -0.59$, $\text{Ps} < 10^{-4}$) in the present data whereas it is only weak ($\text{Rs} = -0.31$, $\text{Ps} = 0.002$) if FWHM $\text{H}\beta$ is compared directly with EW Fe II. Instead, there is a strong

correlation ($R_s = 0.56$, $P_s < 10^{-4}$) between FWHM $H\beta$ and EW $H\beta$. The lack of correlation between the line width and Fe II strength (when measured independently with $H\beta$) in Grupe et al. (1999), Vaughan et al. (2001) and the present work has confirmed that the anti-correlation arises because $H\beta$ gets weaker as the lines get narrower (Osterbrock 1977; Gaskell 1985; Goodrich 1989b; Gaskell 2000).

In addition to our confirmation of well documented correlations between different AGN properties, we report on three newly discovered correlations involving the $H\beta$ redshift (or blueshift), flux ratios of Fe II to $H\beta$ broad component ($Fe\,II/H\beta_b$) and $[O\,III]$ to $H\beta$ narrow component ($[O\,III]/H\beta_n$). The correlations covering $[O\,III]/H\beta_n$ have never been investigated by other authors so far. We find the relative strength of Fe II to $H\beta_b$ ($Fe\,II/H\beta_b$) significantly correlated to both the $H\beta$ redshift⁷ ($R_s = -0.64$, $P_s < 10^{-4}$) and the relative strength of $[O\,III]$ to $H\beta_n$ ($[O\,III]/H\beta_n$, $R_s = -0.60$, $P_s < 10^{-4}$). A correlation test was also applied between $H\beta$ redshift and $[O\,III]/H\beta_n$. The correlation is prominent in our sample ($R_s = -0.38$, $P_s < 3 \times 10^{-4}$). Figure 6 shows the correlations. There is a trend that strong $Fe\,II/H\beta_b$ –weak $[O\,III]/H\beta_n$ objects tend to have blueshifts in $H\beta$ while strong $[O\,III]/H\beta_n$ –weak $Fe\,II/H\beta_b$ objects tend to have redshifts in $H\beta$. These strong correlations between $Fe\,II/H\beta_b$, $H\beta$ redshift and $[O\,III]/H\beta_n$ must reflect some physical connection between broad and narrow line emitting regions.

4. Discussion

One key to understand the central engines of AGN lies in examining their local environment. The standard paradigm proposes that the surrounding gas is photoionized in physically distinct regions by radiation emerging from the central power source(Osterbrock 1989). However, the segregation of the ionized gas into broad-line region (BLR) and narrow-line region (NLR), as well as the details of the gas kinematics are still far from clear. Optical spectroscopy of the ionized gas around galactic nuclei provides strong constraints on the excitation mechanisms. The following discussion addresses three key points: (1) how do the present results compare to previous work; (2) which new correlations do we find and how can we understand them; and (3) which future observations can we perform to distinguish between different suggested scenarios.

⁷A correlation between the $H\beta$ blueshift and flux ratio of Fe II to $H\beta$ whole line was detected in Zheng et al. (2002). We emphasize that our ratio refers to the broad component in $H\beta$ only. Note the sign difference between this paper and Zheng et al. (2002). The positive correlation quoted by Zheng et al. (2002) becomes negative in the notation used herein.

A number of consistent correlations among observational parameters have been searched in order to understand the basic properties underlying the observed spectra. In particular, Boroson & Green (1992) made a landmark study of the optical emission-line properties and continuum properties (radio through X-ray) of 87 low redshift PG quasars. A principal component analysis revealed “eigenvector 1” (EV1) links stronger Fe II emission, weaker [O III] emission from the NLR, and narrower H β (BLR) with stronger line blue asymmetry. More recently, Laor et al. (1997) found these optical properties also go along with steeper soft X-ray spectra and claimed the soft X-ray slope as a related part of EV1. We confirm these trends and present in addition three newly discovered correlations involving the H β redshift, Fe II/H β_b and [O III]/H β_n .

Potentially, EV1 represents a fundamental physical driver that control the energy producing and radiation emitting processes. The two leading interpretations by far are that EV1 is driven by (1) the Eddington ratio L/L_{Edd} (Boroson & Green 1992) and (2) Orientation effect.

Boroson & Green (1992) argued strongly that viewing angle is unlikely to drive EV1, by assuming [O III] emission is isotropic, originating from radii large enough to be free from orientation dependent obscuration. The isotropy of [O III] emission has been questioned by the studies of radio-loud AGN (Hes, Barthel & Fosbury 1993; Baker 1997). However, a recent study of radio-quiet quasars (Kuraszkiewicz 2000) showed a significant correlation between EV1 and orientation independent [O II] emission, which implied that EV1 is not driven by orientation. Moreover, the correlation between [O II] and [O III] emission indicated [O III] emission is not dependent on orientation.

The most promising interpretation at present is that EV1 is mostly governed by L/L_{Edd} (Boroson & Green 1992). This suggestion was based on the notion that the vertical thickness of the accretion disk, driven by the Eddington ratio, controls the line strengths and continuum parameters.

The striking correlations between the H β redshift, Fe II/H β_b and [O III]/H β_n found in the present work give us linkages of the gas kinematics and ionization between BLR and NLR. The question raised is what is the physical process behind the correlations? Can both the new and previous correlations be explained within one single scenario? Indeed, the L/L_{Edd} interpretation provides plausible explanations for the observed trends.

One of the two general scenarios in AGN to explain asymmetric profile is in terms of an outflowing component in the BLR with a change in obscuration by a central disk of clouds on the receding side. Accreting systems in high L/L_{Edd} AGN will drive relatively thick outflows due to their larger photon luminosities per unit gravitational mass. As the velocity of the

outflow increases, the $\text{H}\beta$ develops an increasing excess on the blue wing. The corresponding blue $\text{H}\beta_b$ velocity shift in comparison with $[\text{O III}]$ can be also well predicted because both the line asymmetry and the shift of the line centroids are effects of the same process. The link between BLR and NLR in terms of density is less straight forward to predict. E.g., due to the strong outflow, the NLR might be replaced by denser clouds. Given a typical radial distribution of NLR clouds, $[\text{O III}]/\text{H}\beta_n$ peaks around densities of $\log n = 2\text{--}4$ (e.g., Komossa & Schulz 1997). High-density NLR clouds would therefore lead to a suppression of $[\text{O III}]$ strength. The same is true for the other limit, a low-density NLR. Some authors favored a low-density BLR of NLS1 galaxies (see, e.g., the discussion in Rodriguez-Pascual et al. 1997 and Komossa & Mathur 2001), which may indicate a low-density NLR as well, if both regions are coupled. The best way to measure directly the density of the NLR of NLS1s in the future is to employ the density-sensitive line ratios $[\text{O II}]\lambda 3729/[\text{O II}]\lambda 3726$ or $[\text{S II}]\lambda 6716/[\text{S II}]\lambda 6731$. These ratios are presently generally not reported in the literature. Their measurements requires high S/N spectroscopy and/or resolution to detect and resolve these lines.⁸ More indirectly, other line-ratios will also change in dependence of density and thus allow a density determination. For instance, a higher-density NLR would strongly boost the $[\text{O I}]\lambda 6300$ line (Komossa & Schulz 1997).

Although it is more difficult to illustrate the direct connection between strong Fe II emission and large L/L_{Edd} , some suggestions have been proposed. Pounds et al. (1995) suggested the X-ray spectrum becomes steeper in high L/L_{Edd} AGN. If the EUV–X-ray spectrum plays an important role in the formation and confinement of the BLR clouds (e.g., Krolik, McKee & Tarter 1981), a steep X-ray spectrum coupled to a flatter EUV spectrum will lead to a thicker BLR (e.g., Komossa & Meerschweinchen 2000), and thus stronger Fe II emission if the the low-excitation part of the BLR is mechanically heated (Joly 1987). Increased metal abundances in more extreme NLS1 galaxies (Mathur 2000) would enhance these trends, i.e. lead to thicker BLRs (Komossa et al. 2001). Supersolar iron abundance may additionally boost the strength of Fe II. In another model by Kwan et al. (1995), Fe II line emission is produced in an accretion disk. The AGN with higher L/L_{Edd} might simply have more mass in the accretion disk to produce stronger Fe II emission by postulating collisional excitation (Netzer & Wills 1983; Wills, Netzer & Wills 1985) as the origin of the Fe II emission in general.

The strong correlations of properties linking dynamics (line widths), kinematics (line

⁸We checked the NLR density of the well-measured NLS1 galaxy NGC 4051, using the density-sensitive $[\text{S II}]$ -ratio measured by Veilleux (1991). This yields $\log n \simeq 2.8$ and does not deviate significantly from the values found for, e.g., Seyfert 1 and 2 galaxies. However, NGC 4051 is not an extreme NLS1 in terms of X-ray steepness and Fe II emission.

shifts), ionization in BLR and NLR (Fe II and [O III] strengths), and radiation process (X-ray spectral shape) are likely driven by an intrinsic properties, i.e., the L/L_{Edd} . In order to further test the favored scenario (and get more constraints on, e.g., the density of the NLR), larger and even more complete AGN sample with higher resolution optical data is needed.

5. Summary and Conclusions

This paper presents the statistical study of optical emission line properties of a bright AGN sample selected from RASS. The sample comprises 155 Seyfert 1 type AGN. Our conclusions based on the correlation analysis can be succinctly summarized as follows:

- The previously reported correlations between the strengths of Fe II, [O III] emission and the X-ray slope are confirmed. Strong optical Fe II blends go along with weak forbidden emission lines (e.g., [O III]) and steep X-ray slopes.
- The anti-correlation between the X-ray spectral slope α_X and the FWHM of H β becomes prominent as far as the high luminosity AGN are concerned.
- Striking correlations between the H β redshift, Fe II/H β_b and [O III]/H β_n are found. There is a general trend that strong Fe II/H β_b –weak [O III]/H β_n objects tend to have blueshifts in H β while strong [O III]/H β_n –weak Fe II/H β_b objects tend to have redshifts in H β .
- We add new arguments that the observed trends are likely driven by L/L_{Edd} and describe some future observations that could further test this suggestion.

We thank Drs. Todd A. Boroson and Richard F. Green for providing the Fe II template, Drs. Dirk Grupe, Simon Vaughan, Mira Véron, Philippe Véron, Tinggui Wang, Dieter Engels for helpful discussions on the optical measurements, and the anonymous referee for many useful comments and suggestions. Special thanks go also to the staff at Xinglong station for their instrumental and observing help. D.X. acknowledges a MPG-CAS exchange program. This research has made use of the NASA/IPAC Extragalactic Database (NED), which is operated by the Jet Propulsion Laboratory, Caltech, under contract with the National Aeronautics and Space Administration. The ROSAT project is supported by the Bundesministerium für Bildung und Forschung (BMBF) and the Max-Planck-Gesellschaft. This work was supported by NSFC under grant 19973014.

REFERENCES

Appenzeller, I., Zickgraf, F.J., Krautter, J., & Voges, W. 2000, A&A, 364, 443

Appenzeller, I., Thiering, I., Zickgraf, F.-J., et al. 1998, ApJS, 117, 319

Bade, N., Engels, D., & Voges, W. 1998, A&AS, 127, 145

Bade, N., Fink, H., Engels, D., et al. 1995, A&AS, 110, 469

Baker, J.C. 1997, MNRAS, 286, 23

Boller, Th., Brandt, W.N., & Fink, H. 1996, A&AS, 305, 53

Boroson, T.A., & Green, R.F. 1992, ApJS, 80, 109

Brinkmann, W., & Siebert, J. 1994, A&A, 285, 812

Brotherton, M.S., Wills, B.J., Francis, P.J., & Steidel, C.C. 1994, ApJ, 430, 495

Corbin, M.R. 1995, ApJ, 447, 496

Corbin, M. R., & Boroson, T. A. 1996, ApJS, 107, 69

Corbin, M.R. 1997, ApJS, 113, 245

Creshaw, D.M. 1986, ApJS, 62, 821

de Robertis, M.M. 1985, ApJ, 289, 67

Evans, I.N. 1988, ApJS, 67, 373

Fiore, F., Elvis, M., McDowell J. C., et al. 1994, ApJ, 431, 515

Fischer, J.-U., Hasinger, G., Schwope, A.D., et al. 1998, Astron. Nachr., 319, 347

Francis, P.J., Hewett, P.C., Foltz, C.B., & Chaffee, F.H. 1992, ApJ, 398, 476

Gaskell, C. M. 1982, ApJ, 263, 79

Gaskell, C.M. 1985, ApJ, 291, 112

Gaskell, C.M. 2000, New Astronomy Review, 44, 563

Goodrich, R.W. 1989a, ApJ, 340, 190

Goodrich, R.W. 1989b, ApJ, 342, 224

Grupe, D., Beuermann, K., Thomas, H.-C., Mannheim, K., & Fink H.H. 1998, A&A, 330, 25

Grupe, D., Beuermann, K., Mannheim, K., & Thomas, H.-C. 1999, A&A, 350, 31

Hes, R., Barthel, P.D., & Fosbury, R.A.E. 1993, Nature, 362, 326

Joly, M. 1987, A&A, 184, 33

Komossa, S., Grupe, D., & Janek, M. 2001, in AIP Conf. Proc. 599, X-ray Astronomy '999: stellar endpoints, AGN and the diffuse background, ed. N. White, G. Malaguti, & G. Palumboi, 686

Komossa, S., & Schulz, H. 1997, A&A, 323, 31

Komossa, S., & Mathur, S. 2001, A&A, 374, 914

Komossa, S., & Meerschweinchen, J. 2000, A&A, 354, 411

Krolik, J.H., McKee, C.F., Tarter, C.B. 1981, ApJ, 249, 422

Kuraszkiewicz, J., Wilkes, B.J., Brandt, W.N., et al. 2000, ApJ, 542, 631

Kwan, J., Cheng, F., Fang, L., et al. 1995, ApJ, 440, 628

Laor, A., Bahcall, J. N., Jannuzzi, B.T., Schneider, D.P., & Green, R.F. 1995, ApJS, 99, 1

Laor, A., Fiore, F., Martin, E., et al. 1997, ApJ, 477, 93

Lawrence, A., Elvis, M., Wilkes, B.J., McHardy, I. & Brandt, N. 1997, MNRAS, 285, 879

Massey, P., & Strobel, K. 1988, ApJ, 328, 315

Mathur, S. 2000, MNRAS, 314, L17

McIntosh, D.H., Rix, H.-W., Rieke, M.J., & Foltz, C.B. 1999, ApJ, 517, L73

Miller, P., Rawlings, S., Saunders, R., & Eales, S. 1992, MNRAS, 254, 93

Netzer, H., & Wills, B.J. 1983, ApJ, 275, 445

Oke, J.B., & Lauer, T.R. 1979, ApJ, 230, 360

Osterbrock, D.E. 1977, ApJ, 215, 733

Osterbrock, D.E., & Shuder, J.M. 1982, ApJS, 49, 149

Osterbrock, D.E., & Pogge, R.W. 1985, *ApJ*, 297, 166

Osterbrock, D.E. 1989, *Astrophysics of Gaseous Nebulae and Active Galactic Nuclei* (University Science Books: Mill Valley, CA)

Pounds, K.A., Done, C., Osborne, J.P., 1995, *MNRAS*, 277, L5

Press, W.H., Teukolsky, S.A., Vetterling, W.T., & Flannery, B.P. 1992, *Numerical recipes in FORTRAN: The art of scientific computing* (2nd ed.; Cambridge: University Press)

Phillips, M.M. 1978, *ApJ*, 226, 736

Rodríguez-Ardila, A., Pastoriza, M.G., & Donzelli, C.J. 2000a, *ApJS*, 126, 63

Rodríguez-Ardila, A., Binette, L., Pastoriza, M.G., & Donzelli, C.J. 2000b, *ApJ*, 538, 581

Rodriguez-Pascual P.M., Mas-Hesse J.M., Santos-Lleo M., 1997, *A&A*, 327, 72

Schartel, N., Walter, R., Fink, H.H., et al. 1996, *A&A*, 307, 33

Schwöpe, A.D., Hasinger, G., Lehmann, I., et al. 2000, *Astron. Nachr.*, 321, 1

Stripe, G.M. 1991, *A&A*, 247, 3

Thomas, H.-C., Beuermann, K., Reisch, K., et al. 1998, *A&A*, 335, 467

Tytler, D., & Fan, X.-M. 1992, *ApJS*, 79, 1

Vaughan, S., Edelson, R., Warwick, R.S., et al. 2001, *MNRAS*, 327, 673

Veilleux, S. 1991, *ApJ*, 369, 331

Véron-Cetty, M.P., Véron, P., & Gonçalves, A.C. 2001, *A&A*, 372, 730

Véron-Cetty, M.P., & Véron, P. 2000, *A&A Rev.*, 10, 81

Voges, W., Boller, Th., Dennerl, K., et al. 1996, in *MPE Report 263, Rontgenstrahlung from the Universe*, ed. H.U. Zimmermann, J. Trümper, & H. Yorke, 637

Voges, W., et al. 1999, *A&A*, 349, 389

Wang, T., Brinkmann, W., & Bergeron, J. 1996, *A&A*, 309, 81

Wei, J.Y., Xu, D.W., Dong, X.Y., & Hu, J.Y. 1999, *A&AS*, 139, 575 (Paper I)

Wills, B.J., Brotherton, M.S., Fang, D., Steidel, C.C., & Sargent, W.L.W. 1993, *ApJ*, 415, 563

Wills, B.J., Netzer, H., & Wills, D. 1985, *ApJ*, 288, 94

Wills, B. 1982, in IAU Symp. 97, Extragalactic Radio Sources, ed. D.S. Heeschen & C.M. Wade (Dordrecht: Kluwer), 373

Xu, D.W., Wei, J.Y., & Hu, J.Y. 1999, *ApJ*, 517, 622

Zheng, X.Z., Xia, X.Y., Mao, S., et al. 2002, *AJ*, 124, 18

Zickgraf, F.-J., Thiering, I., Krautter, J., et al. 1997, *A&AS*, 123, 103

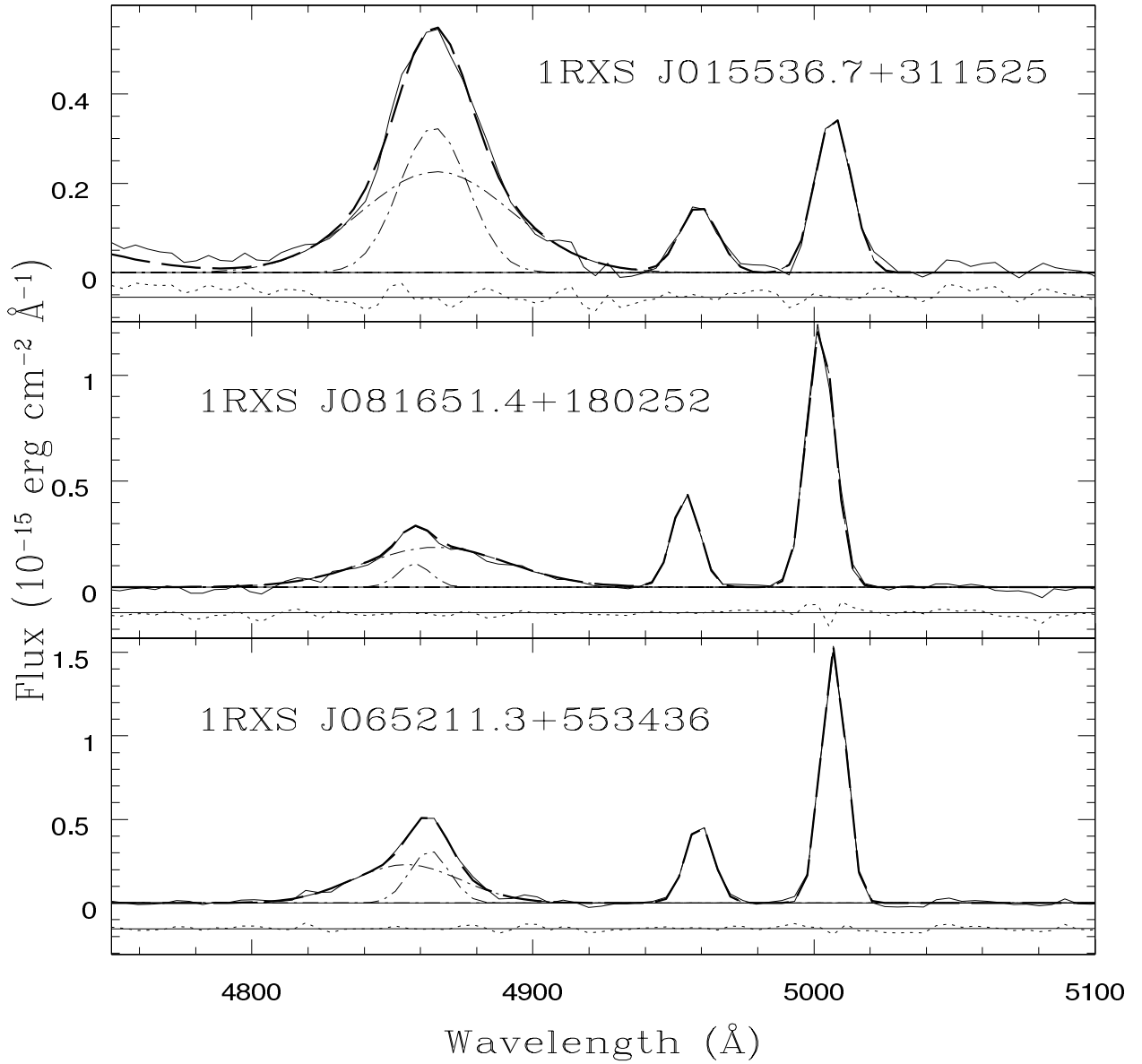


Fig. 1.— Illustration of velocity shift between the broad and narrow Gaussian components of H β . Top panel: For 1RXS J015536.7+311525, H β can be well fitted by a sum of two Gaussian components without velocity difference. Middle panel: For 1RXS J081651.4+180252, H β shows a redshifted broad component relative to the narrow one. Bottom panel: For 1RXS J065211.3+553436, H β can be represented by a blueshifted broad component and a narrow component.

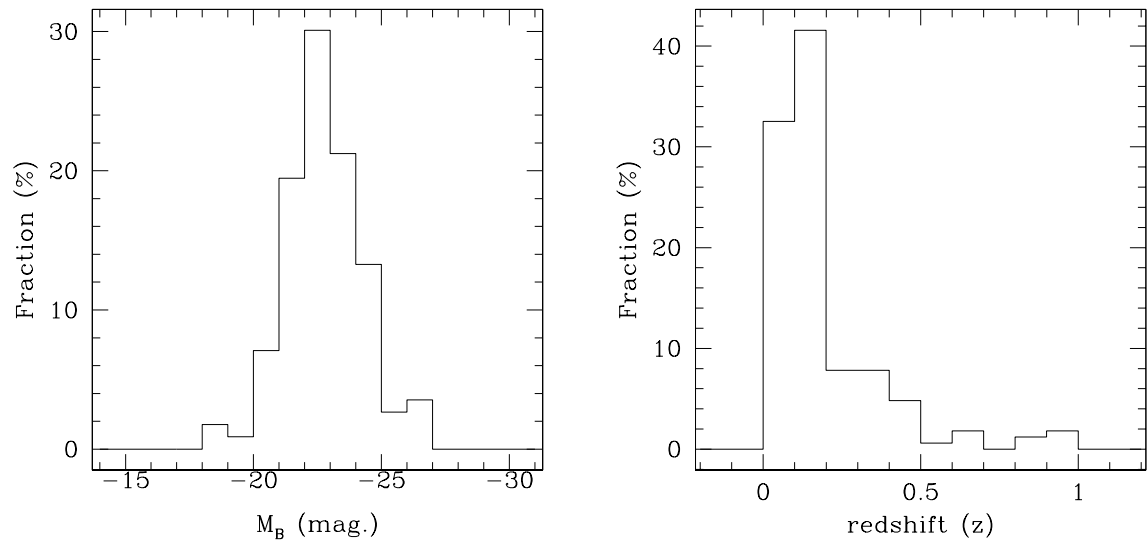


Fig. 2.— Absolute magnitude M_B and redshift distributions of the Seyfert 1 type AGN

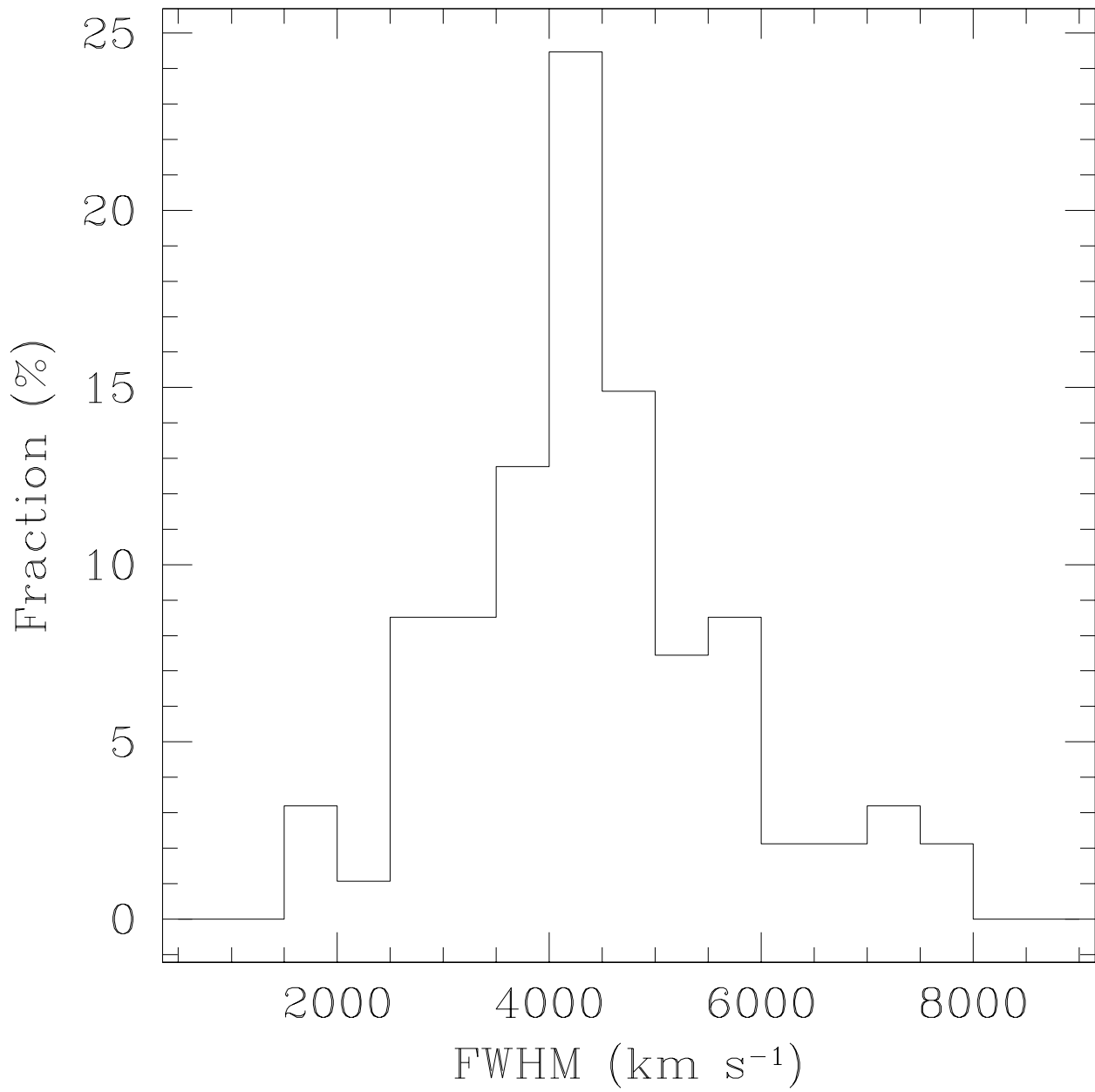


Fig. 3.— Distribution of the FWHM of H β for the Seyfert 1 type AGN

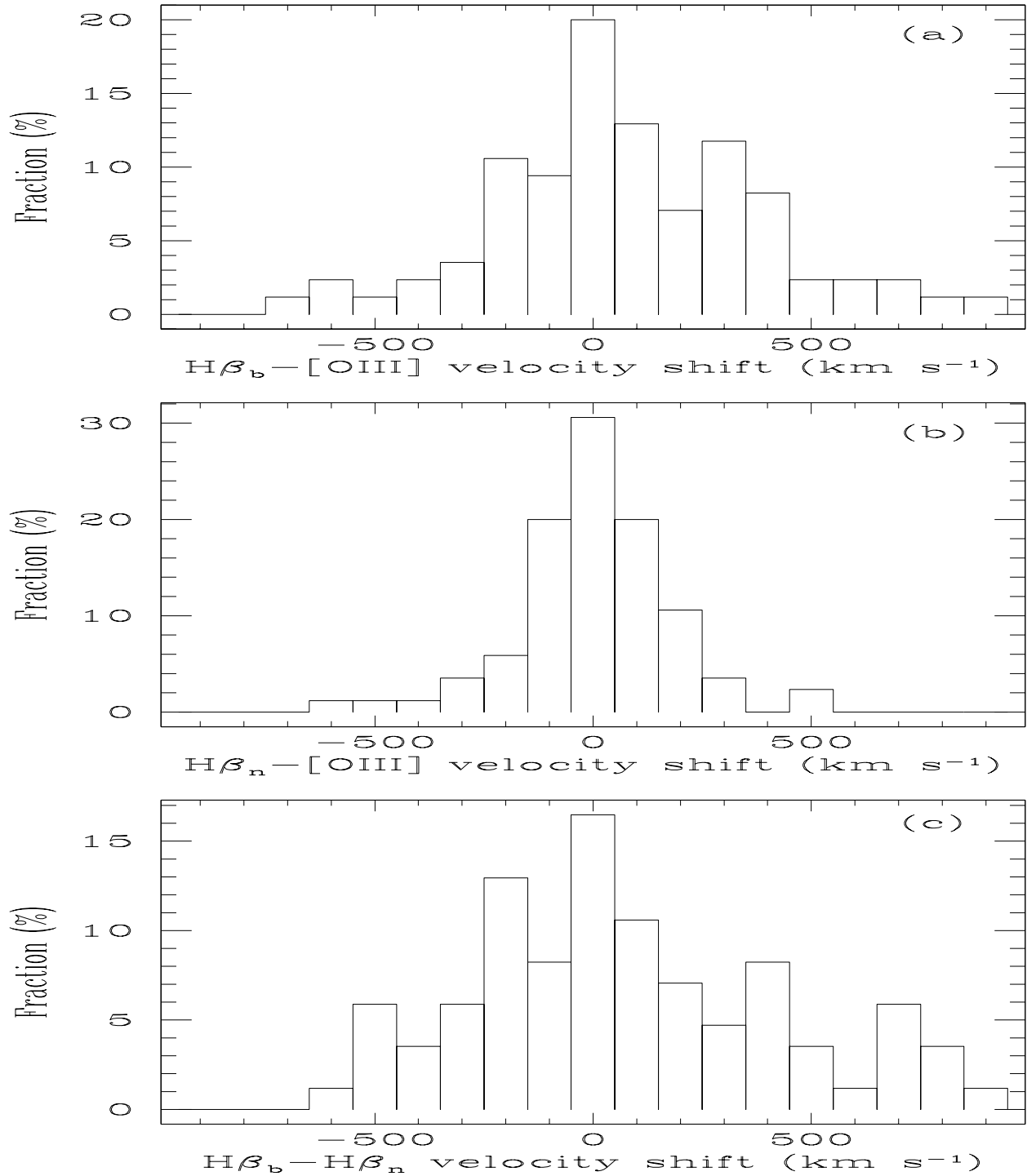


Fig. 4.— Distribution of velocity shifts for $H\beta_b$, $H\beta_n$ and $[\text{O III}]\lambda 5007$

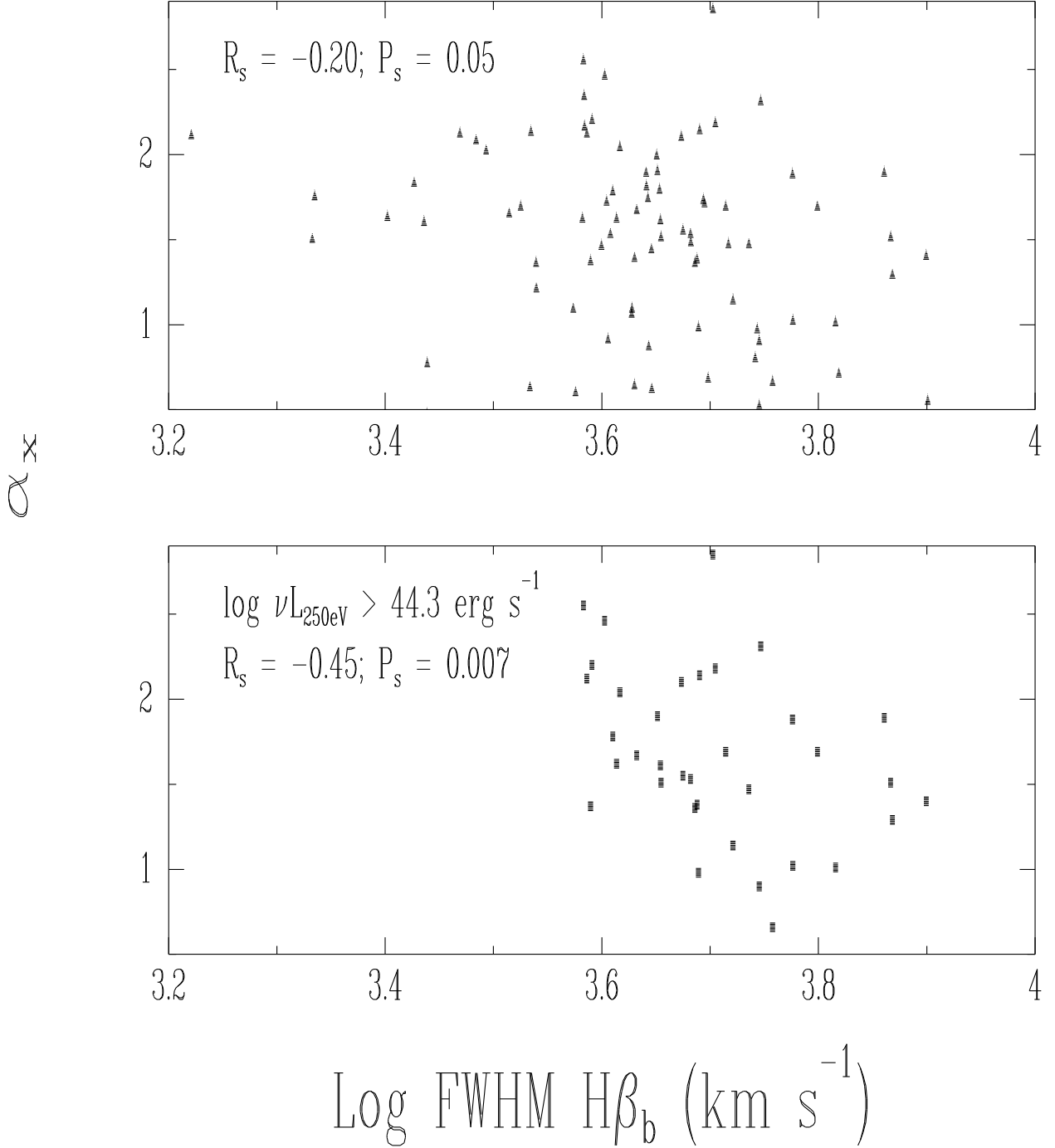


Fig. 5.— The X-ray slope α_X as a function of H β FWHM line widths. The upper graph shows the correlation diagram for the sample, the lower graph for the high-luminosity AGN with $\log \nu L_{250\text{eV}} > 44.3 \text{ erg s}^{-1}$.

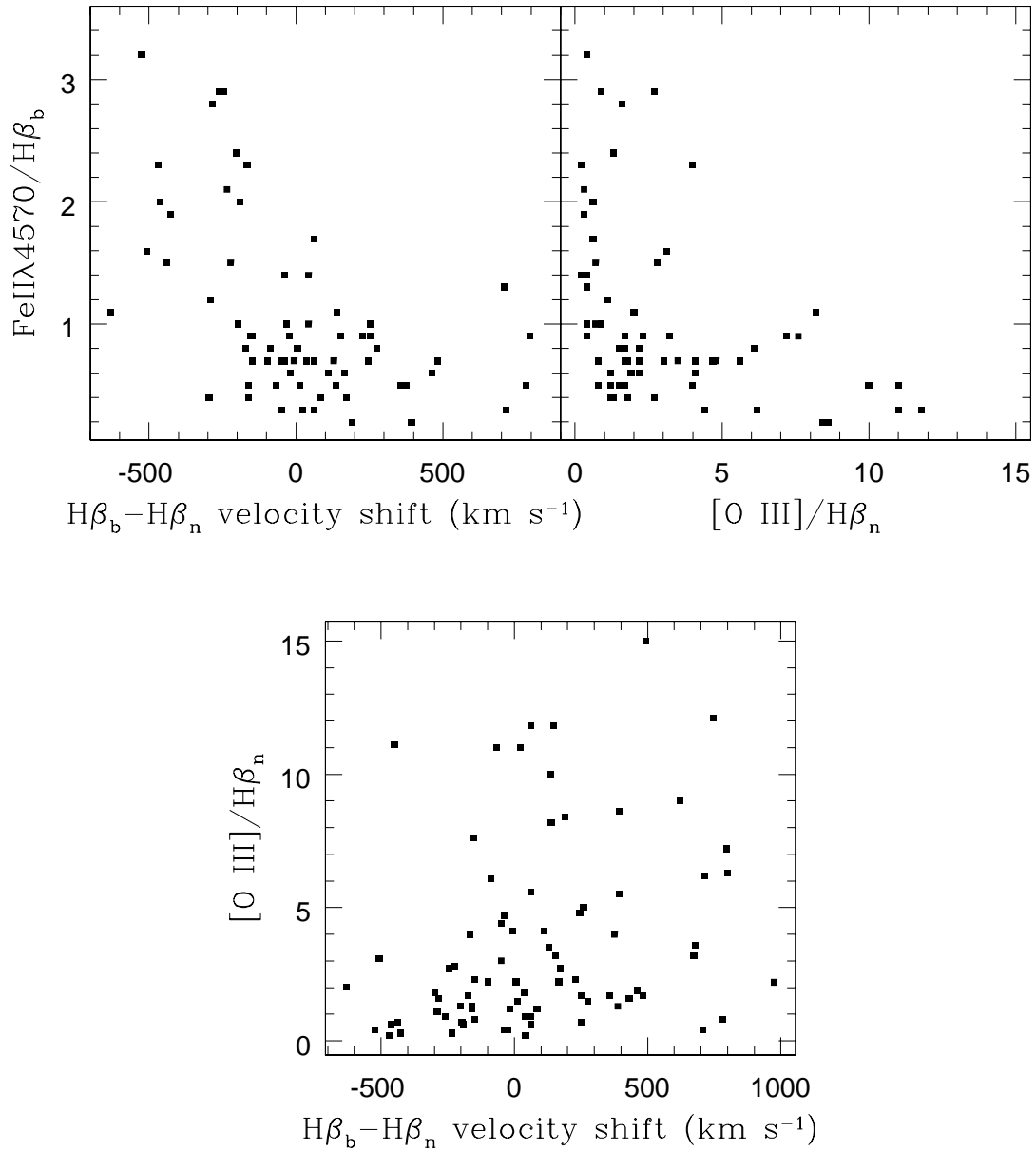


Fig. 6.— Correlation diagrams for $\text{Fe II}\lambda 4570/\text{H}\beta_b$, $\text{H}\beta_b - \text{H}\beta_n$ velocity shift and $[\text{O III}]/\text{H}\beta_n$.

Table 1. Properties of the Seyfert 1 type AGN sample

Name	z	$H\beta_b$ FWHM (km s ⁻¹)	$H\beta_n$	[O III]	$H\beta_b$ EW (Å)	Fe II EW (Å)	[O III]	[O III]/ $H\beta_b$	Fe II/ $H\beta_n$	Δv^a (km s ⁻¹)	Δv^b (km s ⁻¹)	Δv^c (km s ⁻¹)	α_{opt}	α_X	$\log(\nu L_{1/4})$ (erg s ⁻¹)	
1RXS J000011.9+052318	0.040	3050	1050	600	37.3	26.7	22.5	0.6	1.8	0.7	40	-50	-90	1.2	2.08 ± 0.18	43.6
1RXS J000055.5+172346	0.215	6420	2290	830	75.5	64.9	8.5	0.1	0.9	0.9	640	150	-490	0.6	1.73 ± 0.35	44.3
1RXS J000550.0+102249	0.095	4240	-	660	58.6	0.0	45.8	0.8	-	0.0	380	340	-40	2.0	1.06 ± 0.47	43.4
1RXS J000915.0+243758	0.118	3880	1540	640	34.0	13.5	12.9	0.4	2.3	0.4	-70	-150	-80	1.4	1.60 ± 0.43	44.0
1RXS J000953.0+371906	0.154	4240	-	1380	27.6	34.6	22.8	0.8	-	1.3	-	70	-	-	1.84 ± 0.46	44.3
1RXS J001121.2+373919	0.104	3770	1010	860	52.7	38.2	12.4	0.2	1.7	0.7	480	290	-190	-	0.60 ± 0.49	43.5
1RXS J001452.7+270549	0.086	3350	870	760	28.7	25.5	24.4	0.8	2.3	0.9	230	200	-30	1.1	1.69 ± 0.23	43.9
1RXS J002007.2+324423	0.082	3820	1380	950	38.1	78.7	3.6	0.1	0.3	2.1	-230	-260	-30	-	1.62 ± 0.45	43.6
1RXS J002445.3+082047	0.067	1660	690	690	31.0	72.2	6.2	0.2	4.0	2.3	-170	-220	-50	-	2.11 ± 0.50	43.3
1RXS J002811.6+310342 ^d	0.500	-	-	762	-	-	8.8	-	-	-	-	-	-	2.1	1.32 ± 0.25	45.5
1RXS J002902.7+195717	0.264	5720	740	720	71.0	24.7	14.4	0.2	6.2	0.3	720	260	-460	-	0.66 ± 0.63	44.2
1RXS J003121.2+301558	0.200	3940	715	630	23.8	27.2	33.1	1.4	9.9	1.1	-370	-310	60	-	1.99 ± 0.52	44.4
1RXS J003221.1+242359	0.066	3460	1180	620	13.2	38.2	14.1	1.1	0.9	2.9	-260	-230	30	-	1.21 ± 0.33	43.1
1RXS J004459.4+192143	0.179	3900	1380	750	20.3	64.6	9.5	0.5	0.4	3.2	-520	-470	50	0.8	2.20 ± 0.24	44.6
1RXS J005034.2+044152	0.097	1780 ^e	-	-	-	-	-	-	-	-	-	-	-	-	1.88 ± 0.40	43.5
1RXS J005050.6+353645	0.058	5470	2300	1230	48.1	27.3	10.8	0.2	0.5	0.6	160	0	-160	0.7	2.21 ± 0.15	44.0
1RXS J005607.6+254802	0.153	6600	1960	1230	73.3	61.9	13.8	0.2	0.9	0.8	-760	90	850	1.1	1.71 ± 0.39	44.4
1RXS J011655.1+254937	0.099	4000	910	1070	56.4	40.1	43.1	0.8	3.0	0.7	-50	-110	-60	0.0	-	-
1RXS J011745.5+363718	0.107	3770	1720	700	68.3	51.8	17.2	0.3	0.6	0.8	40	230	190	0.7	1.03 ± 0.28	44.0
1RXS J011848.2+383626	0.216	5040	1590	1070	68.0	50.0	13.5	0.2	0.8	0.7	-150	40	190	-	2.85 ± 0.43	44.8
1RXS J012556.6+351039	0.312	6790	-	570	78.3	21.0	12.6	0.2	-	0.3	-	0	-	-	0.86 ± 0.89	44.3
1RXS J012923.0+223100	0.231	4730	980	800	65.7	39.4	17.3	0.3	2.2	0.6	170	0	-170	-	1.55 ± 0.71	44.4
1RXS J013738.5+852414	0.499	4270	-	710	-	-	8.0	0.2	-	-	-	180	-	-	0.80 ± 0.92	44.8
1RXS J014023.0+240255	0.072	4620	1300	1260	48.3	44.0	13.7	0.3	0.9	0.9	-200	-70	130	1.6	1.89 ± 0.37	44.0
1RXS J014025.2+382400	0.067	3110	800	620	72.2	38.2	22.6	0.3	4.0	0.5	380	290	-90	1.7	2.02 ± 0.24	44.0
1RXS J015536.7+311525	0.135	3830	1750	910	24.8	42.6	9.3	0.4	0.6	1.7	60	270	200	0.5	2.34 ± 0.50	44.1
1RXS J015546.4+071902	0.069	3750 ^e	1090 ^e	800	-	-	26.7	-	-	-	-	-	-	0.0	1.22 ± 0.54	43.2
1RXS J015555.6+040620	0.136	6980	2030	750	51.9	63.1	9.9	0.2	1.1	1.2	0	0	0	-	1.15 ± 0.36	43.8
1RXS J015621.6+241838	0.155	3770	940	660	51.5	70.7	18.9	0.4	2.7	1.4	-60	-20	40	-	1.73 ± 0.85	44.3
1RXS J023601.9+082124 ^f	0.228	4390	1250	1230	82.1	74.2	21.2	0.3	1.7	0.9	250	80	-170	-	2.86 ± 0.62	45.5
1RXS J023739.9+181945	0.168	4560	950	850	87.4	58.1	15.8	0.2	5.1	0.7	160	30	-130	0.8	-	-
1RXS J024214.5+074442	0.451	4950	1410	700	59.2	0.0	17.2	0.3	0.9	0.0	60	0	-60	-	1.71 ± 0.78	45.5
1RXS J033522.6+190739	0.189	6180	-	800	30.8	5.8	19.3	0.6	-	0.2	-	200	-	0.9	0.20 ± 0.45	44.2
1RXS J034308.0+185836	0.110	3420	1300	830	75.0	56.5	44.4	0.6	1.5	0.8	280	410	130	1.6	0.63 ± 0.62	43.8
1RXS J035147.6+103618	0.185	5100	1040	910	70.1	0.0	28.9	0.4	7.3	0.0	580	460	-120	1.9	2.54 ± 0.66	45.2

Table 1—Continued

Name	z	$H\beta_b$ FWHM (km s ⁻¹)	$H\beta_n$	[O III]	$H\beta_b$ EW (Å)	Fe II EW (Å)	[O III] EW (Å)	[O III]/ $H\beta_b$	Fe II/ $H\beta_n$	$H\beta_b$	Δv^a (km s ⁻¹)	Δv^b (km s ⁻¹)	Δv^c (km s ⁻¹)	α_{opt}	α_X	$\log(\nu L_{1/4})$ (erg s ⁻¹)
1RXS J035345.9+195825	0.029	3800	1150	710	23.0	14.0	6.4	0.3	1.2	0.6	0	0	0	-	1.73 ± 0.72	43.2
1RXS J040513.2+173647	0.098	3850	-	920	67.9	-	9.0	0.1	-	-	-310	-	-	-	-	-
1RXS J041147.1+132417	0.277	2960	1010	790	49.1	49.5	8.8	0.2	0.4	1.0	-30	170	200	-	3.10 ± 1.07	45.8
1RXS J044428.6+122113	0.089	3140	1320	1280	33.8	106.3	30.5	0.9	1.4	3.1	-490	-250	240	1.2	1.33 ± 0.54	44.0
1RXS J062334.6+644542	0.086	4400	1550	990	53.0	0.0	117.3	2.2	3.6	0.0	680	490	-190	2.0	0.87 ± 0.38	43.8
1RXS J065136.5+563732	0.286	4810	1320	670	52.0	55.5	13.8	0.3	2.0	1.1	-630	-680	-50	-	1.53 ± 0.59	44.6
1RXS J065211.3+553436	0.064	2750	1010	620	25.8	40.3	39.4	1.5	3.1	1.6	-510	-400	110	-	0.47 ± 0.46	43.1
1RXS J071006.0+500243	0.154	4030	1600	620	43.7	60.4	7.3	0.2	0.2	1.4	40	250	210	0.0	0.91 ± 0.58	44.1
1RXS J071339.7+382043	0.123	4140	1200	700	58.0	102.5	17.0	0.3	0.7	1.8	-490	-340	150	0.5	1.33 ± 0.46	44.0
1RXS J071858.2+705920	0.066	4810	1310	850	20.3	57.7	38.2	1.9	1.6	2.8	-280	-250	30	-	1.48 ± 0.32	43.2
1RXS J071923.7+570840	0.175	6540	1150	960	102.7	0.0	81.4	0.8	3.2	0.0	670	560	-110	0.2	1.01 ± 0.33	44.3
1RXS J072220.6+732041	0.350	3570	1320	820	59.7	76.4	10.6	0.2	0.7	1.3	-150	300	450	-	2.71 ± 0.35	45.1
1RXS J072408.4+355309	0.138	7260	820	680	94.4	0.0	74.0	0.8	11.1	0.0	-450	-510	-60	0.6	1.89 ± 0.18	44.7
1RXS J072826.6+303407	0.100	3980	1010	600	59.7	48.1	15.3	0.3	2.2	0.8	0	0	0	1.4	1.46 ± 0.53	43.7
1RXS J072912.9+410552	0.103	4460	1580	1040	47.6	41.6	29.4	0.6	3.7	0.9	-230	190	420	-	1.28 ± 0.39	43.8
1RXS J073308.7+455511	0.142	8070	3240	930	58.1	48.9	16.7	0.3	0.3	0.8	-440	-190	250	0.1	1.28 ± 0.29	44.5
1RXS J073735.8+430856	0.119	4500	670	660	33.8	-	51.7	1.5	14.9	-	0	0	0	-	-	-
1RXS J074228.1+465648	0.170	4050	-	620	99.3	69.3	25.4	0.3	-	0.7	-	330	-	1.4	-	-
1RXS J074311.3+742926	0.332	7380	1060	840	94.0	32.1	31.4	0.3	4.4	0.3	-50	-140	-90	-	1.29 ± 0.26	44.9
1RXS J074759.2+205229	0.156	5540	820	690	71.7	48.7	12.4	0.2	3.5	0.7	130	70	-60	1.2	0.97 ± 0.45	44.0
1RXS J074906.2+451039	0.192	4500	800	800	100.4	55.1	80.4	0.8	8.4	0.6	0	0	0	0.4	0.04 ± 0.84	43.6
1RXS J075026.6+270726	0.154	-	-	-	-	-	-	-	-	-	-	-	-	-	1.01 ± 0.38	43.7
1RXS J075039.5+624205	0.194	6300	1330	1500	58.5	18.0	22.3	0.4	11.0	0.3	20	-90	-110	0.9	1.69 ± 0.36	44.4
1RXS J075408.7+431611	0.350	-	-	570	-	-	31.5	-	-	-	-	-	-	-	1.38 ± 0.30	45.0
1RXS J075409.5+512436	0.331	3680	-	730	99.0	108.2	11.0	0.1	-	1.1	-	0	-	-	-	-
1RXS J075634.7+362232 ^g	0.884	-	-	-	-	-	-	-	-	-	-	-	-	-	1.60 ± 0.42	45.8
1RXS J075910.0+115152	0.050	4470	1180	700	25.9	52.8	12.7	0.5	0.6	2.0	-190	-190	0	1.4	1.99 ± 0.32	43.3
1RXS J080132.3+473618	0.157	7840	-	900	119.0	69.7	13.1	0.1	-	0.6	-530	-190	340	0.4	1.29 ± 0.17	44.6
1RXS J080358.9+433248	0.451	5580	1340	670	75.6	0.0	38.4	0.5	1.3	0.0	390	570	180	-	2.31 ± 0.32	45.3
1RXS J080534.6+543132	0.406	5780	1530	730	51.5	-	30.1	0.6	1.5	-	-370	-250	120	-	2.01 ± 0.22	45.5
1RXS J080548.5+112617	0.144	4480	880	770	89.6	0.0	50.0	0.6	5.0	0.0	260	0	-260	0.7	1.90 ± 0.22	44.2
1RXS J080639.9+724831	0.099	1760	740	820	13.7	34.4	61.9	4.5	6.2	2.5	-190	-220	-30	0.7	1.25 ± 0.34	43.7
1RXS J080727.2+140534	0.074	2450	-	-	51.7	70.2	<20	<0.4	-	1.4	-	0	-	-	0.98 ± 0.45	43.3
1RXS J081237.9+435636	0.183	4110	-	700	51.5	21.6	11.8	0.2	-	0.4	-	-90	-	0.4	1.14 ± 0.44	44.2
1RXS J081502.4+525304	0.126	4110	1080	770	75.8	41.2	14.7	0.2	1.7	0.5	360	230	-130	0.2	1.62 ± 0.24	44.2

Table 1—Continued

Name	z	H β_b FWHM (km s $^{-1}$)	H β_n [O III] (Å)	H β_b EW (Å)	Fe II EW (Å)	[O III] H β_b EW (Å)	[O III]/ H β_b H β_n	Fe II/ H β_b	Δv^a (km s $^{-1}$)	Δv^b (km s $^{-1}$)	Δv^c (km s $^{-1}$)	α_{opt}	α_X	$\log(\nu L_{1/4})$ (erg s $^{-1}$)		
1RXS J081651.4+180252	0.158	3890	810	700	68.4	0.0	84.6	1.2	9.0	0.0	620	680	60	0.9	1.37±0.20	44.5
1RXS J081718.6+520200	0.040	2170 ^e	470	-	-	25.2	-	-	-	-	-	-	-	1.09±0.42	42.6	
1RXS J081738.0+242333	0.283	5560	960	740	73.0	14.9	125.4	1.7	8.6	0.2	390	350	-40	-	0.90±0.74	44.3
1RXS J082633.1+074259	0.312	3460	1010	880	50.0	65.6	6.0	0.1	1.3	1.3	-130	310	440	-	-	-
1RXS J082942.2+415442	0.126	7960	800	910	70.1	0.0	98.6	1.4	12.1	0.0	750	700	-50	1.8	0.55±0.39	43.5
1RXS J083737.3+254746	0.080	-	-	960	0.0	-	13.3	-	-	-	-	-	-	-	-	-
1RXS J083820.6+241025	0.043	4980	780	750	26.0	18.0	11.0	0.0	3.0	0.0	-680	-770	-90	-	1.70±0.29	43.2
1RXS J084026.2+033316	0.060	4940	1510	990	55.6	0.0	28.5	0.5	1.6	0.0	430	390	-40	0.3	1.73±0.21	43.6
1RXS J084302.0+030226	0.512	1920	-	-	53.1	43.3	-	-	-	0.8	-	-	-	-	2.25±0.38	45.4
1RXS J084622.3+031318	0.107	4380	1000	960	71.6	49.7	24.2	0.3	4.1	0.7	0	-150	-150	0.9	1.81±0.26	44.1
1RXS J084856.8+584150	0.134	-	-	890	-	0.0	23.3	-	-	-	-	-	-	-	1.29±0.47	43.7
1RXS J084918.7+531806	0.112	2750	810	990	23.3	20.6	29.7	1.3	7.6	0.9	-150	-20	130	1.5	0.77±0.48	43.2
1RXS J085233.3+422539	0.137	2670	750	700	14.8	43.3	22.8	1.5	2.7	2.9	-250	-220	30	1.1	1.83±0.38	43.9
1RXS J085358.8+770054	0.106	5480	2300	620	23.1	40.8	11.7	0.5	0.8	1.8	-640	-540	100	1.6	1.34±0.16	43.8
1RXS J085443.8+401912	0.152	5520	1100	810	60.6	37.1	19.7	0.3	1.9	0.6	460	440	-20	1.8	0.80±0.30	43.7
1RXS J085706.2+621050	0.160	-	-	-	-	-	-	-	-	-	-	-	-	-	0.08±0.97	43.4
1RXS J085820.6+642100	0.115	3060 ^e	1260 ^e	970	-	-	63.7	-	-	-	-	-	-	-	1.18±0.40	43.6
1RXS J085902.0+484611	0.083	4420	1300	910	80.0	72.2	36.1	0.5	2.3	0.9	-150	-130	20	0.6	1.44±0.11	44.1
1RXS J190910.3+665222	0.191	3830	600	670	97.0	111.7	7.0	0.1	1.1	1.2	-290	-40	250	0.9	2.55±0.12	44.8
1RXS J193929.8+700752	0.116	4850	1690	1160	60.9	54.1	14.1	0.2	0.4	0.9	-20	80	100	0.2	1.36±0.15	44.4
1RXS J210550.5+041435	0.139	-	-	-	-	-	-	-	-	-	-	-	-	-	1.54±0.54	43.9
1RXS J212654.3+112403	0.096	2730	1600	1120	66.7	33.3	14.1	0.2	0.8	0.5	780	350	-430	0.7	1.60±0.28	44.1
1RXS J214309.6+153658	0.385	7610	-	1230	72.7	0	10.9	0.1	-	0	-	120	-	-	1.00±0.94	44.9
1RXS J214655.2+092102 ^g	0.984	-	-	-	-	-	-	-	-	-	-	-	-	-	0.83±0.61	45.6
1RXS J215912.7+095247	0.102	5380	-	1110	71.4	26.0	50.0	0.7	-	0.4	-	0	-	1.3	1.51±0.25	44.2
1RXS J221537.8+290239	0.229	5980	600	640	70.0	0.0	54.5	0.8	11.8	0.0	150	220	70	-	1.02±0.36	44.4
1RXS J221918.8+120757	0.082	2080 ^e	-	-	-	-	-	-	-	-	-	-	-	-	2.58±0.22	44.4
1RXS J222537.5+225917	0.173	2150	1100	1100	52.5	39.4	17.8	0.3	4.7	0.7	-40	0	40	0.6	1.50±0.47	44.0
1RXS J222846.3+333500	0.090	3270	900	1260	44.4	24.1	46.1	1.0	11.0	0.5	-70	0	70	-	1.65±0.73	44.0
1RXS J222934.3+305720	0.319	7930	1390	1110	88.0	0.0	30.0	0.3	6.3	0.0	800	900	100	-	1.40±0.43	44.8
1RXS J223019.5+163114	0.084	4270	1740	1310	55.8	34.9	17.2	0.3	1.2	0.6	-20	80	100	0.8	1.39±0.31	43.8
1RXS J224621.7+314206	0.145	-	-	660	0	-	25.3	-	-	-	-	-	-	-	1.48±0.30	44.4
1RXS J224939.6+110016	0.084	4390	1440	1220	24.7	47.2	3.5	0.1	0.3	1.9	-430	-180	250	0.9	1.74±0.25	44.0
1RXS J225148.5+341937	0.132	3050	1120	590	51.4	55.5	10.5	0.2	0.6	1.1	40	220	180	0.6	1.43±0.22	44.5
1RXS J225209.6+264236	0.069	2160	700	700	16.7	39.4	15.5	0.9	1.3	2.4	-200	-200	0	1.3	1.75±0.26	43.7

Table 1—Continued

Name	z	$H\beta_b$ FWHM (km s ⁻¹)	$H\beta_n$	[O III]	$H\beta_b$ EW (Å)	Fe II EW (Å)	[O III] EW (Å)	[O III]/ $H\beta_b$	Fe II/ $H\beta_n$	$H\beta_b$	Δv^a (km s ⁻¹)	Δv^b (km s ⁻¹)	Δv^c (km s ⁻¹)	α_{opt}	α_X	$\log(\nu L_{1/4})$ (erg s ⁻¹)
1RXS J225639.4+261846	0.176	-	-	-	-	-	-	-	-	-	-	-	-	0.87±0.79	43.8	
1RXS J230328.0+144341	0.080	-	-	-	-	-	-	-	-	-	-	-	-	0.20±0.46	42.9	
1RXS J231456.0+224325	0.171	3750	1230	1170	62.8	127.8	22.4	0.4	0.7	2.0	-360	-360	0	0.9	0.98±0.35	44.1
1RXS J231517.5+182825	0.104	3310	1190	1200	25.0	18.3	10.7	0.4	6.4	0.7	0	0	0	-	-	-
1RXS J232554.6+215310	0.120	5260	950	770	125.2	0.0	62.5	0.5	5.5	0.0	390	330	-60	1.1	1.14±0.13	44.5
1RXS J232841.4+224853	0.129	5400	-	810	121.7	0.0	34.6	0.3	-	0.0	-	0	-	1.5	1.10±0.54	43.7
1RXS J234728.8+242743	0.159	4270	2550	1350	105.1	0.0	75.2	0.7	2.2	0.0	980	770	-210	1.7	0.64±0.17	44.2
1RXS J234734.6+271910 ^g	0.646	-	-	-	-	-	-	-	-	-	-	-	-	-	-	-
1RXS J235152.7+261938	0.040	3750	1850	1460	47.7	19.0	36.7	0.8	1.8	0.4	-300	-250	50	0.9	1.09±0.21	43.3
1RXS J235754.3+132418	0.115	4290	2000	1480	102.3	101.9	35.5	0.3	0.9	1.0	40	380	340	1.5	1.67±0.18	44.2
III ZW 2	0.090	4990	700	630	72.1	33.3	47.1	0.7	10.0	0.5	140	0	-140	0.5	0.68±0.24	44.0
4C 25.01	0.284	4310	1050	840	74.6	79.1	38.8	0.5	8.2	1.1	140	140	0	-	1.51±0.43	44.9
PG 0026+12	0.142	4890	1120	690	36.1	19.2	14.8	0.4	1.5	0.5	0	360	360	0.9	0.98±0.13	44.5
S 10785	0.134	5970	1290	850	89.1	65.4	26.2	0.3	5.6	0.7	60	260	200	1.5	1.88±0.21	44.6
MARK 1148	0.064	5560	840	800	135.3	22.8	55.0	0.4	8.4	0.2	190	290	100	1.2	0.52±0.16	43.5
PG 0052+251	0.155	5110	780	780	68.8	19.2	30.0	0.4	8.6	0.3	60	20	-40	0.6	1.38±0.18	44.9
B2 0110+29	0.363	7360	680	750	77.6	0.0	63.1	0.8	15.0	0.0	490	520	30	-	1.51±0.63	44.8
3C 48.0	0.367	4080	1840	1200	31.0	46.2	37.2	1.2	2.8	1.5	-220	270	490	0.3	1.78±0.11	45.9
MS 02448+1928	0.176	4510	2000	780	70.0	59.5	23.9	0.3	1.1	0.9	780	720	-60	-	1.93±0.77	44.7
MS 03574+1046	0.182	4160	1660	890	42.2	72.2	13.0	0.3	0.5	1.7	-380	-90	290	1.1	2.73±1.10	45.3
RX J04506+0642	0.118	3460	1150	940	22.5	45.2	11.0	0.5	0.6	2.0	-460	-360	100	0.7	1.36±1.11	44.0
MS 07007+6338	0.152	5070	2070	840	49.8	63.6	8.4	0.2	0.4	1.3	710	450	-260	0.2	2.18±0.33	44.4
VII ZW 118	0.079	4910	2300	860	58.1	71.4	14.3	0.2	0.5	1.2	490	680	190	0.5	1.95±0.09	44.7
F07144+4410	0.061	3820	1380	830	95.8	65.3	105.1	0.8	2.4	0.7	-120	-70	50	0.7	1.16±0.21	44.1
MS 07199+7100	0.125	4020	1330	680	54.8	50.9	26.3	0.5	7.2	0.9	800	230	-570	-	1.72±0.23	44.1
RX J07491+2842	0.345	4710	820	620	84.3	57.7	12.3	0.1	4.8	0.7	250	140	-100	-	2.10±0.39	44.7
RX J07527+2617	0.082	2940	1060	780	38.3	55.0	7.9	0.2	0.4	1.4	-40	-40	0	-	2.12±0.23	44.0
B3 0754+394	0.096	3840	1430	870	57.3	46.8	38.1	0.7	1.7	0.8	-170	-130	40	0.6	2.16±0.33	43.9
KUV 07549+4228 ^f	0.210	4620	1520	780	57.5	74.2	48.5	0.8	2.4	1.3	170	70	-100	0.3	2.14±0.22	44.9
PG 0804+761	0.100	5490	2380	950	65.4	85.1	11.3	0.2	0.3	1.3	-300	-60	240	-0.2	1.30±0.07	44.7
RX J08297+3252	0.127	3420	820	710	33.7	30.9	44.2	1.3	3.2	0.9	150	150	0	1.3	2.13±0.42	43.9
RX J08307+3405	0.063	4500	1090	680	37.7	21.6	36.9	1.0	4.1	0.6	110	140	30	1.6	1.79±0.26	43.6
US 1329	0.249	5180	1280	760	112.4	48.2	55.8	0.5	2.7	0.4	170	120	-50	-	1.69±0.15	45.2
VII ZW 244	0.131	4510	2000	770	60.1	88.0	15.2	0.3	0.7	1.5	-440	-190	250	0.8	1.61±0.17	44.2
KUV 08482+4146	0.134	4130	-	740	62.2	39.4	11.4	0.2	-	0.7	-	-520	-	1.2	1.47±0.26	44.0

Table 1—Continued

Name	z	$H\beta_b$	$H\beta_n$	[O III]	$H\beta_b$	Fe II	[O III]	[O III]/ $H\beta_b$	Fe II/ $H\beta_b$	Δv^a	Δv^b	Δv^c	α_{opt}	α_X	$\log(\nu L_{1/4})$	
		FWHM			EW	EW	EW	$H\beta_b$	$H\beta_n$	(km s ⁻¹)					(erg s ⁻¹)	
		(km s ⁻¹)			(Å)	(Å)	(Å)									
MARK 1220	0.064	4050	770	930	30.7	23.9	25.8	0.8	6.1	0.8	-90	140	220	-	1.53±0.31	43.5
4C 73.18	0.303	5670	1770	870	53.6	0.0	10.3	0.2	0.6	0.0	-60	50	110	-	1.02±0.16	45.1
RX J20389+0303 ^f	0.137	4410	1410	750	65.5	67.7	31.3	0.3	0.7	1.0	40	-100	-140	1.3	1.81±0.74	44.1
S5 2116+81	0.086	4130	-	740	122.7	22.5	92.6	0.8	-	0.2	-	0	-	1.8	0.71±0.14	44.0
MS 21283+0349	0.094	4900	1330	660	105.4	50.9	54.8	0.5	2.5	0.5	-370	-310	60	0.4	2.14±0.22	44.6
II ZW 136	0.063	3770	980	760	81.4	72.5	17.4	0.2	0.9	0.9	250	120	-130	0.9	2.46±0.13	44.7
MS 22102+1827	0.079	2950	870	900	27.3	68.9	6.2	0.1	0.3	2.5	-120	-120	0	1.3	2.49±0.27	44.0
RX J22186+0802	0.120	2530	780	810	22.5	36.1	23.7	1.1	3.5	1.6	-140	90	220	1.6	-	-
RX J22198+0935	0.060	2520	910	740	15.1	7.9	11.4	0.8	1.2	0.5	-160	-100	60	-	1.63±0.45	43.1
PG 2233+134	0.325	4750	1340	740	41.1	67.8	10.4	0.3	0.4	1.7	-570	-410	160	-	0.90±0.62	44.3
AKN 564	0.025	3860	970	720	31.6	23.1	50.6	1.6	2.2	0.7	-100	-150	-50	1.4	2.12±0.04	44.5
KUV 22497+1439	0.135	4140	1560	1040	47.5	110.1	4.2	0.1	0.2	2.3	-470	0	470	0.6	2.04±0.20	44.5
RX J2256.6+0525	0.065	4240	1230	730	82.9	37.0	53.5	0.6	1.3	0.4	-160	-50	110	1.1	1.09±0.20	43.8
KAZ 320	0.034	4430	1230	830	48.3	17.8	53.8	1.1	1.2	0.4	90	220	130	1.3	0.62±0.12	43.1
RX J23171+0838	0.165	5440	910	690	85.7	21.1	31.1	0.4	10.1	0.2	250	60	-190	0.7	1.47±0.37	44.2

^a $H\beta$ broad component velocity shift with respect to narrow component. A positive velocity indicates a redshift of $H\beta$ broad component with relative to narrow component, whereas a negative velocity refers to a blueshift.

^b $H\beta$ broad component velocity shift relative to the systemic frame. A positive velocity corresponds to a redward shift of $H\beta$ broad component with respect to systemic, while a negative velocity represents a blueshift.

^c $H\beta$ narrow component velocity shift relative to the systemic frame. A positive velocity corresponds to a redward shift of $H\beta$ narrow component with respect to systemic, while a negative velocity represents a blueshift.

^d $H\beta$ is weak.

^e $H\beta$ FWHM measurements are based on the $H\alpha$.

^fSources show obvious asymmetric [O III] $\lambda\lambda$ 4959, 5007 profiles

^g $H\beta$ and [O III] are not in the observed wavelength range.

Note. — The Prefix of the object name indicates the origin of sources. ‘1RXS J’ represents the source that was identified as emission line AGN in our identification program, while other prefix refer to the known AGN that meet our selection criteria. The typical uncertainty of the the emission line fluxes is about 10-20%. Errors for FWHM and velocity shift measurements are \lesssim 150 km s⁻¹.

Table 2. Spearman Rank-Order Correlation Coefficient Matrix

Property	(1)	(2)	(3)	(4)	(5)	(6)	(7)	(8)	(9)	(10)	(11)	(12)
(1)FWHM(H β_b)	–	0.002	0.032	-0.32 (0.0020)	0.35 (0.0009)	-0.59 (0.0000)	-0.05	0.34 (0.001)	-0.20	-0.04	0.38 (0.0003)	0.48 (0.0000)
(2)FWHM(H β_n)	–	0.46 (0.0000)	0.30 (0.004)	-0.263	0.23	-0.294 (0.005)	-0.15	0.23	-0.104	-0.66 (0.0000)	0.11	
(3)FWHM([OIII])	–	-0.03	0.004	-0.02	-0.08	0.02	-0.06	-0.166	-0.15	-0.01		
(4)EW FeII			–	-0.59 (0.0000)	0.81 (0.0000)	-0.546 (0.0000)	-0.471 (0.0000)	0.41 (0.0001)	-0.129	-0.544 (0.0000)	0.06	
(5)EW [OIII]				–	-0.64 (0.0000)	0.73 (0.0000)	0.33 (0.0019)	-0.39 (0.0002)	0.195	0.67 (0.0000)	0.05	
(6)FeII/H β_b					–	-0.23 (0.0000)	-0.64 (0.0011)	0.34	-0.055	-0.60 (0.0000)	0.24	
(7)[OIII]/H β_b						–	0.009	-0.33 (0.0017)	0.27	0.45 (0.0000)	-0.314 (0.0038)	
(8) Δv^a							–	-0.24	0.147	0.375	0.14 (0.0003)	
(9) α_X								–	-0.236	-0.37 (0.0004)	0.36 (0.001)	
(10) α_{opt}									–	0.109	-0.29 (0.0069)	
(11)[OIII]/H β_n										–	0.1	
(12)Log νL_{250eV}											–	

^avelocity shift between broad and narrow Gaussian components of H β in units of km s⁻¹.